
This is the **accepted version** of the article:

Yin, Gaofei; Verger, Alexandre; Filella, Iolanda; [et al.]. «Divergent estimates of forest photosynthetic phenology using structural and physiological vegetation indices». *Geophysical Research Letters*, Vol. 47, issue 18 (Sep. 2020), e2020GL0891672020. DOI 10.1029/2020GL089167

This version is available at <https://ddd.uab.cat/record/232631>

under the terms of the  **CC BY** COPYRIGHT license

Divergent Estimates of Forest Photosynthetic Phenology Using Structural and Physiological Vegetation Indices

Gaofei Yin^{1, 2, 3}, Alexandre Verger^{2, 3}, Iolanda Filella^{2, 3}, Adrià Descals^{2, 3} and Josep Peñuelas^{2, 3}

¹Faculty of Geosciences and Environmental Engineering, Southwest Jiaotong University, Chengdu 610031, China, ²CREAF, Cerdanyola del Vallès 08193, Catalonia, Spain, ³CSIC, Global Ecology Unit, Cerdanyola del Vallès 08193, Catalonia, Spain

Corresponding author: G. Yin (g.yin@creaf.uab.cat)

Key Points:

- Structural and physiological regulations of plant carbon uptake determine forest photosynthetic phenology
- Structural vegetation indices successfully identified the start of season for deciduous forests
- Physiological vegetation indices tracked the best evergreen forest photosynthetic phenology and the end of season for deciduous forests

Abstract

The accurate estimation of photosynthetic phenology using vegetation indices (VIs) is important for measuring the interannual variation of atmospheric CO₂ concentrations, but the relative performances of structural and physiological VIs remain unclear. We found that structural VIs (normalized difference vegetation index, enhanced vegetation index, and near-infrared reflectance of vegetation) were suitable for estimating the start of the photosynthetically active season in deciduous broadleaf forests using gross primary production measured by FLUXNET as a benchmark, and a physiological VI (chlorophyll/carotenoid index) was better at identifying the end of the photosynthetically active season for deciduous broadleaf forests and both the start and end of season for evergreen needleleaf forests. The divergent performances were rooted in the combined control of structural and physiological regulations of carbon uptake by plants. Most existing studies of photosynthetic phenology have been based on structural VIs, so we suggest revisiting the dynamics of photosynthetic phenology using physiological VIs, which has significant implications on global plant phenology and carbon uptake studies.

Plain Language Summary

The uptake of photosynthetic carbon by forests is strongly seasonal, which can be characterized by photosynthetic phenology, e.g. the start and end of the photosynthetically active season (SOS and EOS, respectively). Satellite vegetation indices (VIs) can detect photosynthesis in canopies either structurally or physiologically. Clarifying the convergence or divergence of the performance of structural and physiological VIs is therefore crucial. This study compared the capacity of three structural VIs and one physiological VI for estimating SOS and EOS. Their performances were jointly controlled by structural and physiological regulations of carbon uptake by plants. The structural and physiological controls for deciduous broadleaf forests (DBFs) were nearly synchronous during green-up, and canopy structural changes were visible, so structural VIs were reliable for estimating SOS. Canopies, however, change slowly in evergreen needleleaf forests (ENFs) throughout the year and in DBFs during autumn, and the capacity to take up carbon is mainly limited by physiological stress, so physiological VIs outperformed structural VIs. Our study highlights the unique advantage of physiological VIs for estimating photosynthetic phenology. These findings constitute a step toward improving our understanding of the roles of the structural and physiological regulations of the dynamics of terrestrial carbon.

1. Introduction

Forests account for approximately four billion ha (~30%) of the terrestrial surface and offset the abundant anthropogenic CO₂ emissions (Bonan, 2008). The uptake of photosynthetic carbon by forests is strongly seasonal, which substantially influences the interannual variation of atmospheric CO₂ concentrations (Xia *et al.*, 2015). A better understanding of the timing of photosynthetic activity, i.e. photosynthetic phenology, is therefore necessary for improving models of the global terrestrial ecosystem and for more accurately predicting future cycles of climate–carbon feedbacks (Peaucelle *et al.*, 2019; Verger *et al.*, 2015).

The rate of carbon uptake by plants can be represented as the product of absorbed photosynthetically active radiation (APAR) and photosynthetic light-use efficiency (LUE) (Garbulsky *et al.*, 2011; Penuelas *et al.*, 2011). APAR determines the potential photosynthetic rate and is mainly controlled by canopy structure (Running *et al.*, 2004). The potential photosynthetic rate, however, is often downregulated by environmental stresses, so LUE was introduced to

quantify how much of this potential is actually realized (Penuelas *et al.*, 2011). Environmental stresses can induce plant physiological responses, and excess APAR is dissipated by several photoprotective mechanisms, e.g. chlorophyll fluorescence emission and heat dissipation, which are remotely detectable (Demmig-Adams and Adams, 2000; Garbulsky *et al.*, 2014).

Satellite vegetation indices (VIs) have been widely used in recent decades to identify photosynthetic phenology and its response to climate change (Chang *et al.*, 2019; D’Odorico *et al.*, 2015; Gonsamo *et al.*, 2012; Middleton *et al.*, 2016; Wu *et al.*, 2017). The information contents of existing VIs can be categorized into structure and physiology. Structural VIs mainly represent vegetation biomass, with typical examples including the normalized difference vegetation index (NDVI), enhanced vegetation index (EVI) and near-infrared reflectance of vegetation (NIRv). NDVI and EVI may be the most widely used VIs and are strongly correlated with APAR (Huete *et al.*, 2002). NIRv accounts for the influence of background brightness and quantifies the near-infrared reflectance of terrestrial vegetation (Badgley *et al.*, 2017). NIRv scales well with *in situ* eddy covariance measurements of CO₂ flux at monthly and longer time scales (Badgley *et al.*, 2019) because of its sensitivity to structure (Kimm *et al.*, 2020). Physiological VIs such as the photochemical reflectance index (PRI) were designed to characterize plant physiology. PRI represents both the diurnal activity of the xanthophyll cycle and seasonal changes to chlorophyll/carotenoid pigment ratios (Penuelas *et al.*, 1994; Wong and Gamon, 2015b), and has been extensively demonstrated to adequately estimate LUE (Garbulsky *et al.*, 2011; Penuelas *et al.*, 2011; Zhang *et al.*, 2017).

To the best of our knowledge, most, if not all, studies that have extracted photosynthetic phenology using VIs have relied on structural VIs. These VIs only measure potential photosynthetic rates, overlooking actual rates, so erroneous results are expected. For example, the start of the photosynthetically active season (SOS) for deciduous forests has often been estimated to be later than it was (Jeong *et al.*, 2017; Marien *et al.*, 2019), and both SOS and the end of the photosynthetically active season (EOS) for evergreen forests cannot be accurately estimated using structural VIs (Wu *et al.*, 2017). The main challenge of using physiological VIs, e.g., PRI, to track photosynthetic phenology is the limited availability of the key bands for calculating them. For example, the 531 nm wavelength, which can detect changing pigment levels during the dissipation of heat due to excess APAR (Wong and Gamon, 2015a; b), is specified as an ocean band, and some preprocessing (e.g. atmospheric correction) is not operationally implemented by MODIS products. The calculation of PRI from satellite data sets is therefore time consuming, hindering its wide application for monitoring photosynthetic phenology.

The recent update of the MODIS reflectance product using the Multi-Angle Implementation of Atmospheric Correction (MAIAC) algorithm has allowed the easy acquisition of surface reflectance for both terrestrial and ocean bands across large areas and at high frequencies of observation (Lyapustin *et al.*, 2012). The advent of this product offers promising prospects for tracking photosynthetic phenology using PRI. MODIS is not equipped with the reference band in the original PRI formula and alternative bands have been selected to calculate “MODIS PRI” (Goerner *et al.*, 2009; He *et al.*, 2016; Middleton *et al.*, 2016). The “MODIS PRI” calculated from bands 1 and 11 is more closely linked to the seasonal change in chlorophyll/carotenoid pigments than to the daily xanthophyll cycle, and it was recently referred to as the chlorophyll/carotenoid index (CCI) (Gamon *et al.*, 2016).

Structural and physiological VIs can theoretically provide complementary information about photosynthetic activity based on LUE paradigm: the structural VIs represent potential

photosynthetic rates, and the physiological VIs characterize the short-term downregulation of the maximum LUE, thus providing a measure of the extent to which the potential is realized under stress (Penuelas *et al.*, 2011). Our understanding of the unique advantages of each VI for estimating photosynthetic phenology and the differences in their performance across different forest types (e.g. deciduous and evergreen) for different phenological indicators (e.g. SOS and EOS), however, is still very limited. To fill this knowledge gap, we assessed and compared the performance of three structural VIs (NDVI, EVI and NIRv) and one physiological VI (CCI) to extract SOS and EOS for forest photosynthetic activity. All four VIs were calculated using MAIAC reflectance. *In situ* gross primary productivity (GPP) at the sites of eddy-flux towers in ENFs and DBFs was used as a benchmark to validate the VI-derived photosynthetic phenologies.

2. Materials and Methods

2.1. FLUXNET data

We selected 33 ENF and 18 DBF sites with eddy-flux towers from the FLUXNET-2015 data set (available at <http://fluxnet.fluxdata.org/data/fluxnet2015-dataset/>) (Table S1). Detailed information for each site can be found in the supporting information. Sites were selected based on the criteria: (1) they were in the Northern Hemisphere with latitudes $>30^\circ$ (see **Figure S1**) and (2) had at least five years of concomitant *in situ* GPP and MODIS observations during 2001-2014.

The GPPs in the FLUXNET-2015 data set were calculated using gap-filled data for net ecosystem exchange and the standard flux-partitioning method (Lasslop *et al.*, 2010). We used the GPPs from the nighttime-based approach (Reichstein *et al.*, 2005), where nighttime data were used to parameterize a respiration model that was then applied to the entire data set to estimate ecosystem respiration. GPP was then calculated as the difference between ecosystem respiration and net ecosystem exchange.

2.2. MODIS vegetation indices

The VIs were calculated using surface reflectance from the MCD19A1 Version 6 product. This product was generated using the MAIAC algorithm, which uses an adaptive time series and spatial analysis to derive atmospheric aerosol concentration and surface reflectance without empirical assumptions (Lyapustin *et al.*, 2012). MCD19A1 provides daily surface reflectance for MODIS bands 1-12 at spatial resolutions of 1 km.

The time series of the MCD19A1 observations were first extracted at the closest pixel to each selected FLUXNET site for comparison with *in situ* GPP measurements. Pixels contaminated by cloud, snow or a high aerosol optical depth were then excluded based on the layer of quality assurance of the data set. Data with viewing zenith angles $>40^\circ$ were also excluded to minimize the effects of the bidirectional reflectance distribution function (BRDF) (Middleton *et al.*, 2016; Wang *et al.*, 2020).

We analyzed the potentials of NDVI, EVI, NIRv and CCI to characterize SOS and EOS. These VIs were calculated as:

$$NDVI = \frac{B_2 - B_1}{B_2 + B_1} \quad (1)$$

$$EVI = \frac{2.5(B_2 - B_1)}{B_2 + 6B_1 - 7.5B_3 + 1} \quad (2)$$

$$NIR_v = B_2 \frac{B_2 - B_1}{B_2 + B_1} \quad (3)$$

$$CCI = \frac{B_{11} - B_1}{B_{11} + B_1} \quad (4)$$

where B1, B2, B3 and B11 are surface reflectances in MODIS bands 1 (620–670 nm), 2 (841–876 nm), 3 (459–479 nm) and 11 (526–536 nm), respectively. A scaled CCI (sCCI) was calculated to obtain only positive CCI values that compared better with other VIs (Rahman *et al.*, 2004):

$$sCCI = (CCI + 1) / 2 \quad (5)$$

2.3 Extraction of SOS and EOS

Remotely sensed phenologies using VIs are often biased by the effects of snow (Gonsamo *et al.*, 2012; Jin *et al.*, 2017). Snow generally causes abnormal VI values. All VI values during winter (January, February and December) were therefore assigned as the 5% percentile of all available high-quality VIs during winters. This “fixed-winter” preprocessing was proposed by (Beck *et al.*, 2006) and can greatly reduce the effects of snow (Miao *et al.*, 2013).

Time series of *in situ* GPP and the VIs were smoothed using a double logistic function:

$$O_s = O_b + \frac{O_m}{1 + \exp(-c(t - p))} - \frac{O_m + O_b - O_e}{1 + \exp(-d(t - q))} \quad (6)$$

where O_s is the smoothed observation, t is the date (day of year), O_b and O_e are observations (GPP or VIs) before spring green-up and after senescence, respectively, c and d are the slopes of the first and second inflection points associated with forest growth and recession speed, respectively, p and q are the dates of the two inflection points and O_m is the maximum observation at the peak of growth. The parameters (O_b , O_e , c , d , p , q and k) were fitted against real observations using least squares.

Two methods were adopted to extract SOS and EOS, and the first is the dynamic-threshold method. *In situ* smoothed GPP and VIs were normalized using:

$$O_n = \frac{O_s - O_{\min}}{O_{\max} + O_{\min}} \quad (7)$$

where O_n is the normalized observation, O_s is the smoothed observation using the double logistic function (Eq. 6) and O_{\min} and O_{\max} are the minimum and maximum smoothed observations, respectively. SOS and EOS were defined as the days of the year when O_n crossed a threshold. In this study, we specified the dynamic threshold as 0.2, because it is a commonly used threshold and performs well in the most of cases (Shen *et al.*, 2014).

The method proposed by (Gonsamo *et al.*, 2013) (hereafter referred to as Gonsamo’s method) was also employed. Gonsamo’s method analytically estimates the SOS and EOS based on the minima and maxima of the first, second and third derivatives, i.e.,

$$SOS = p + 4.562/2O_b \quad (8)$$

$$EOS = q + 4.562/2O_m \quad (9)$$

where p , q , O_b and O_m are fitted parameters in Eq. (6).

Note that the quality flag of MAIAC is very strict (Lyapustin *et al.*, 2012), which results in low number of high-quality VI observations. We only selected reliable SOS and EOS estimations, such that the number of high-quality observations in a 20-days window around the SOS or EOS are larger than 2 (at least, one before and one after the SOS/EOS). This post-processing reduced the number of SOS and EOS estimates, but assured the reliability of the results.

3. Results

Whilst with slightly different statistics, SOS and EOS from dynamic-threshold and Gonsamo's methods exhibited very similar patterns. Therefore, for simplicity, we only show here the results from dynamic-threshold method, and the results from the Gonsamo's method can be found in the Supporting Information (Figure S2 and S3 for DBFs and ENFs, respectively).

SOS and EOS over the DBF sites derived from NDVI, EVI, NIRv, and sCCI were compared with those derived from *in situ* GPP (see **Figure 1**). SOS derived from *in situ* GPP was accurately estimated by all four VIs, albeit with systematically earlier estimates (bias <0). NIRv estimated SOS for DBFs the best, with the highest R^2 (0.70) and the smallest RMSE (9.57 d) and bias (-2.95 d). In contrast, the performance of NDVI was less satisfactory ($R^2 = 0.60$, RMSE = 13.14 d and bias = -7.54 d). EVI and sCCI provided intermediate accuracy values with slightly lower R^2 (0.69 and 0.67, respectively) and higher RMSEs (10.98 and 10.37 d, respectively) and biases (-4.95 and -4.65 d, respectively) than for NIRv. The VI-detected EOSs were less correlated with their GPP counterparts ($R^2 \leq 0.27$) than were the VI-detected SOS. Estimates of EOS were systematically delayed for all four VIs, but the delay was much shorter for sCCI (3.37 d) than for the other three VIs (≥ 15.39 d). R^2 (0.27) was higher and RMSE (12.19 d) was smaller for sCCI than the three structural VIs, demonstrating its potential for estimating GPP-derived EOS for the DBFs. Among the three structural VIs, NIRv and EVI performed comparably, with both much better than NDVI.

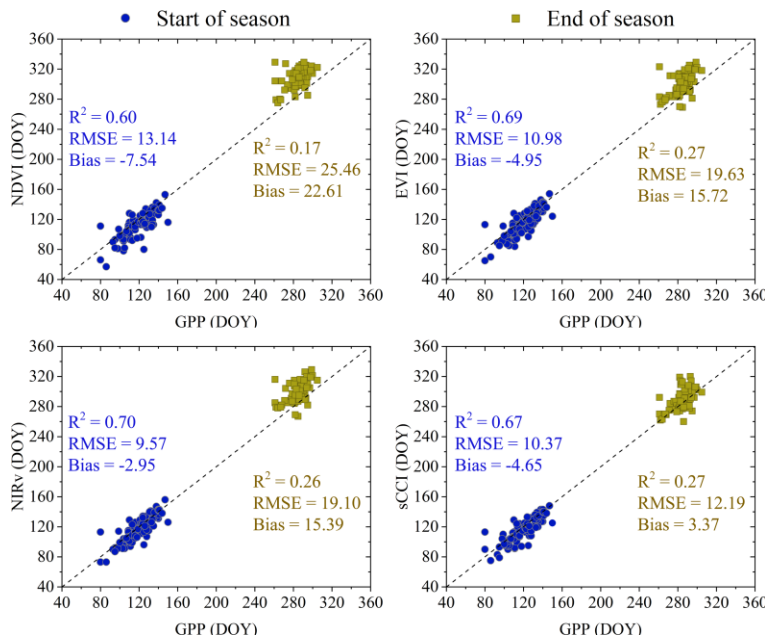


Figure 1. Scatterplots of the dates of the start of the photosynthetically active season (SOS, blue circles) and the end of the photosynthetically active season (EOS, yellow squares) estimated using the vegetation indices and *in situ* gross primary production (GPP) for deciduous broadleaf forests. SOS and EOS were extracted from dynamic-threshold method (Eq. (7)). Statistics are also shown in the figures with blue and yellow texts for SOS and EOS, respectively. DOY: day of year.

Estimates of VI-derived SOS were systematically delayed over the ENF sites (**Figure 2**). The physiological VI (i.e., sCCI in this study), resulted in the smallest RMSE (16.61 d) and bias (9.78 d), confirming its overwhelming performance over the three structural VIs. Similarly, the sCCI-

based EOS estimates over the ENF sites correlated the best with GPP ($R^2 = 0.42$) and had the smallest RMSE (17.69 d).

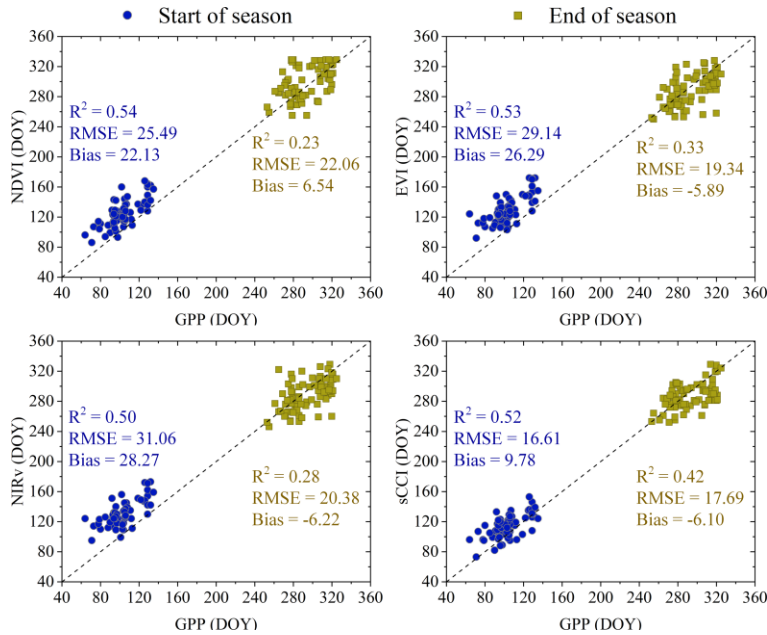


Figure 2. Scatterplots of the dates of the start of the photosynthetically active season (SOS, blue circles) and the end of the photosynthetically active season (EOS, yellow squares) estimated using the vegetation indices and *in situ* gross primary production (GPP) for evergreen needleleaf forests. SOS and EOS were extracted from dynamic-threshold method (Eq. (7)). Statistics are also shown in the figures with blue and yellow texts for SOS and EOS, respectively. DOY: day of year.

4. Discussion

The three structural VIs all estimated earlier SOSs over the DBF sites, as also reported by Fu *et al.* (2014) and Jeong *et al.* (2017). These earlier estimates were most obvious for NDVI (bias = -7.54 d), due to its high sensitivity to understories. Greening in deciduous forests is often first observed at ground level, e.g. herbs and shrubs, so SOS estimated from NDVI mainly indicates the onset of greening of the understory rather than the trees (Ryu *et al.*, 2014). EVI and NIRv were insensitive to background influences (Badgley *et al.*, 2017; Huete *et al.*, 2002) but had a slightly negative bias (-4.95 and -2.95 d, respectively), because trees require time to increase productivity after foliar unfolding, i.e. the timing of carbon assimilation lags behind structural change in deciduous forests (Kikuzawa, 2003). Contrarily, EOS for the DBF sites was later for the structural VIs compared with GPP, consistent with previous studies (Jeong *et al.*, 2017; Marien *et al.*, 2019). This occurs because photosynthesis in high-latitude northern deciduous forests is mainly stressed by photoperiod, although autumnal leaf fall is affected by temperature variability, causing photosynthesis to end before structural recession (Jeong *et al.*, 2017; Medvigy *et al.*, 2013). Structural VIs are widely used for detecting gradual morphological changes in vegetation, even though ENFs have relatively stable amounts of foliage seasonally. NDVI, EVI and NIRv are therefore not recommended for detecting the seasonality of GPP in evergreen forests (Gamon *et al.*, 2016; Wang *et al.*, 2020; Wong *et al.*, 2019; Wu *et al.*, 2017) because the derived SOSs and EOSs are highly uncertain (**Figure 2**).

CCI can detect the physiological dynamics of GPP, unlike the structural VIs. Previous studies have reported that CCI was strongly correlated with the size of the pigment pool (Gamon *et al.*, 2016; Wong *et al.*, 2019), which is an important determiner of LUE and ultimately influences photosynthesis (Croft *et al.*, 2017). The capacity of CCI to track subtle seasonal variations in physiology, specifically the chlorophyll/carotenoid ratio, was confirmed on both foliar (Wong *et al.*, 2019) and canopy (Gamon *et al.*, 2016; Wang *et al.*, 2020) scales. Our study, for the first time,

demonstrated the promising potential of CCI to extract photosynthetic metrics of phenology, especially for those with gradual structural variation, e.g. EOS for DBFs and both SOS and EOS for ENFs.

Forest GPP is simultaneously controlled by its capacities to absorb PAR and to convert APAR into fixed carbon (Penuelas *et al.*, 2011). APAR, representing potential photosynthetic rate, is mainly controlled by forest structure so can be well characterized by structural VIs. Potential photosynthetic rates, however, are often downregulated, which can be tracked by the physiological VIs (Demmig-Adams and Adams, 2000). The structural and physiological controls of the capacity of DBF plants to take up carbon in spring are nearly synchronous, but canopy structural changes are more “visible” from remotely sensed observations (Gamon *et al.*, 2016), so structural VIs are more reliable for estimating SOS for DBFs, especially those insensitive to background influences (e.g. NIRv). The structural recession of DBFs in autumn, however, is gradual, and the photosynthetic rate is mainly controlled by physiology (Gallinat *et al.*, 2015), so EOS for DBFs is detected better by the physiological VIs, e.g., CCI, than by the structural VIs. The canopy structure of evergreens is relatively stable throughout the year, and the dynamics of GPP are mainly determined by physiological constraints (Gamon *et al.*, 2016; Wong and Gamon, 2015b). Physiological VIs may therefore be best for ENFs.

Solar- induced chlorophyll fluorescence (SIF) is also a widely used physiological proxy for tracking GPP dynamics (Jeong *et al.*, 2017; Walther *et al.*, 2016). It is deemed to be directly linked to photosynthetic activity (Porcar-Castell *et al.*, 2014). For example, a recent study demonstrated its high accuracy in capturing EOS (Zhang *et al.*, 2020). Therefore, the comparison between SIF and other VIs is imperative especially for the evergreen species, e.g., tropical forests, for which it is hard to extract their phenology. The temporal and spatial resolutions of satellite-observed SIF are very coarse, which makes the direct comparison between them difficult, whilst the advent of reconstructed SIF from MODIS data (Zhang *et al.*, 2018) provides a new opportunity to compare the performance between SIF and other VIs.

The structural VIs are also influenced by physiology (Badgley *et al.*, 2019), and physiological VIs are similarly confounded by canopy structure (Middleton *et al.*, 2016). Pioneering studies have separated the structural and physiological components to obtain more “pure” spectral observations (Hilker *et al.*, 2011; Zeng *et al.*, 2019), which can be potentially used to decouple the structural/physiological influence from physiological/structural VIs. The estimation of photosynthetic phenology is expected to be further improved if such “pure” structural or physiological VIs are adopted.

5. Conclusions

The capacities of structural (NDVI, EVI and NIRv) and physiological (CCI) VIs calculated using MAIAC reflectances for estimating forest photosynthetic phenology were assessed and compared over 51 forest sites with eddy-flux towers. Results showed that structural VIs are more suitable for estimating the SOS for DBFs, and the physiology-related CCI is better at identifying the EOS for DBFs and both the SOS and EOS for ENFs. The combined control of structural and physiological regulations on carbon uptake by plants is underlying the divergence.

Our study highlights the unique advantage of CCI over existing structural VIs for estimating photosynthetic phenology, especially for ENFs and EOS for DBFs. Most of the existing trending and attributing studies of photosynthetic phenology have relied on structural VIs. Revisiting global

photosynthetic phenology using CCI is therefore necessary, and this will also improve our understanding of the roles of the structural and physiological regulation of global GPP dynamics.

Acknowledgments

This study was supported by the European Union's Horizon 2020 research and innovation programme under the Marie Skłodowska-Curie grant agreement No 835541. *In situ* observations of fluxes were obtained from the FLUXNET 2015 data set (<http://fluxnet.fluxdata.org/data/fluxnet2015-dataset/>). The MCD19A1 C6 product is available online (<https://ladsweb.modaps.eosdis.nasa.gov/search/>). The authors would like to also acknowledge the financial support from the European Research Council Synergy grant ERC-SyG-2013-610028 IMBALANCE-P to JP.

References

- Badgley, G., C. B. Field, and J. A. Berry (2017), Canopy near-infrared reflectance and terrestrial photosynthesis, *Science advances*, 3(3), e1602244.
- Badgley, G., L. D. L. Anderegg, J. A. Berry, and C. B. Field (2019), Terrestrial gross primary production: Using NIRV to scale from site to globe, *Glob Chang Biol*, 25(11), 3731-3740.
- Beck, P. S. A., C. Atzberger, K. A. Høgda, B. Johansen, and A. K. Skidmore (2006), Improved monitoring of vegetation dynamics at very high latitudes: A new method using MODIS NDVI, *Remote Sensing of Environment*, 100(3), 321-334.
- Bonan, G. B. (2008), Forests and climate change: Forcings, feedbacks, and the climate benefits of forests, *Science*, 320(5882), 1444-1449.
- Chang, Q., X. Xiao, W. Jiao, X. Wu, R. Doughty, J. Wang, L. Du, Z. Zou, and Y. Qin (2019), Assessing consistency of spring phenology of snow-covered forests as estimated by vegetation indices, gross primary production, and solar-induced chlorophyll fluorescence, *Agricultural and Forest Meteorology*, 275, 305-316.
- Croft, H., J. M. Chen, X. Luo, P. Bartlett, B. Chen, and R. M. Staebler (2017), Leaf chlorophyll content as a proxy for leaf photosynthetic capacity, *Glob Chang Biol*, 23(9), 3513-3524.
- D'Odorico, P., A. Gonsamo, C. M. Gough, G. Bohrer, J. Morison, M. Wilkinson, P. J. Hanson, D. Gianelle, J. D. Fuentes, and N. Buchmann (2015), The match and mismatch between photosynthesis and land surface phenology of deciduous forests, *Agricultural and Forest Meteorology*, 214-215, 25-38.
- Demmig-Adams, B., and W. W. Adams, 3rd (2000), Harvesting sunlight safely, *Nature*, 403(6768), 371, 373-374.
- Fu, Y. S. H., S. L. Piao, M. Op de Beeck, N. Cong, H. F. Zhao, Y. Zhang, A. Menzel, and I. A. Janssens (2014), Recent spring phenology shifts in western Central Europe based on multiscale observations, *Global Ecology and Biogeography*, 23(11), 1255-1263.
- Gallinat, A. S., R. B. Primack, and D. L. Wagner (2015), Autumn, the neglected season in climate change research, *Trends in ecology & evolution*, 30(3), 169-176.
- Gamon, J. A., K. F. Huemmrich, C. Y. Wong, I. Ensminger, S. Garrity, D. Y. Hollinger, A. Noormets, and J. Penuelas (2016), A remotely sensed pigment index reveals photosynthetic phenology in evergreen conifers, *Proceedings of the National Academy of Sciences of the United States of America*, 113(46), 13087-13092.
- Garbulsky, M. F., I. Filella, A. Verger, and J. Penuelas (2014), Photosynthetic light use efficiency from satellite sensors: From global to Mediterranean vegetation, *Environ Exp Bot*, 103, 3-11.
- Garbulsky, M. F., J. Peñuelas, J. Gamon, Y. Inoue, and I. Filella (2011), The photochemical reflectance index (PRI) and the remote sensing of leaf, canopy and ecosystem radiation use efficiencies: A review and meta-analysis, *Remote Sensing of Environment*, 115(2), 281-297.
- Goerner, A., M. Reichstein, and S. Rambal (2009), Tracking seasonal drought effects on ecosystem light use efficiency with satellite-based PRI in a Mediterranean forest, *Remote Sensing of Environment*, 113(5), 1101-1111.
- Gonsamo, A., J. M. Chen, and P. D'Odorico (2013), Deriving land surface phenology indicators from CO₂ eddy covariance measurements, *Ecological Indicators*, 29, 203-207.
- Gonsamo, A., J. M. Chen, D. T. Price, W. A. Kurz, and C. Wu (2012), Land surface phenology from optical satellite measurement and CO₂ eddy covariance technique, *Journal of Geophysical Research*, 117(G3).
- He, M., J. S. Kimball, S. Running, A. Ballantyne, K. Guan, and F. Huemmrich (2016), Satellite detection of soil moisture related water stress impacts on ecosystem productivity using the MODIS-based photochemical reflectance index, *Remote Sensing of Environment*, 186, 173-183.

Hilker, T., et al. (2011), Inferring terrestrial photosynthetic light use efficiency of temperate ecosystems from space, *Journal of Geophysical Research*, 116(G3).

Huete, A., K. Didan, T. Miura, E. P. Rodriguez, X. Gao, and L. G. Ferreira (2002), Overview of the radiometric and biophysical performance of the MODIS vegetation indices, *Remote Sensing of Environment*, 83(1-2), 195-213.

Jeong, S.-J., D. Schimel, C. Frankenberg, D. T. Drewry, J. B. Fisher, M. Verma, J. A. Berry, J.-E. Lee, and J. Joiner (2017), Application of satellite solar-induced chlorophyll fluorescence to understanding large-scale variations in vegetation phenology and function over northern high latitude forests, *Remote Sensing of Environment*, 190, 178-187.

Jin, H., A. M. Jönsson, K. Bolmgren, O. Langvall, and L. Eklundh (2017), Disentangling remotely-sensed plant phenology and snow seasonality at northern Europe using MODIS and the plant phenology index, *Remote Sensing of Environment*, 198, 203-212.

Kikuzawa, K. (2003), Phenological and morphological adaptations to the light environment in two woody and two herbaceous plant species, *Functional Ecology*, 17(1), 29-38.

Kimm, H., et al. (2020), Deriving high-spatiotemporal-resolution leaf area index for agroecosystems in the U.S. Corn Belt using Planet Labs CubeSat and STAIR fusion data, *Remote Sensing of Environment*, 239, 111615.

Lasslop, G., M. Reichstein, D. Papale, A. D. Richardson, A. Arneeth, A. Barr, P. Stoy, and G. Wohlfahrt (2010), Separation of net ecosystem exchange into assimilation and respiration using a light response curve approach: critical issues and global evaluation, *Global Change Biology*, 16(1), 187-208.

Lyapustin, A. I., Y. Wang, I. Laszlo, T. Hilker, F. G. Hall, P. J. Sellers, C. J. Tucker, and S. V. Korkin (2012), Multi-angle implementation of atmospheric correction for MODIS (MAIAC): 3. Atmospheric correction, *Remote Sensing of Environment*, 127, 385-393.

Marien, B., M. Balzarolo, I. Dox, S. Leys, M. J. Lorene, C. Geron, M. Portillo-Estrada, H. Abdelgawad, H. Asard, and M. Campioli (2019), Detecting the onset of autumn leaf senescence in deciduous forest trees of the temperate zone, *The New phytologist*, 224(1), 166-176.

Medvigy, D., S. J. Jeong, K. L. Clark, N. S. Skowronski, and K. V. R. Schafer (2013), Effects of seasonal variation of photosynthetic capacity on the carbon fluxes of a temperate deciduous forest, *Journal of Geophysical Research-Biogeosciences*, 118(4), 1703-1714.

Miao, L. J., Y. B. Luan, X. Z. Luo, Q. Liu, J. C. Moore, R. Nath, B. He, F. Zhu, and X. F. Cui (2013), Analysis of the Phenology in the Mongolian Plateau by Inter-Comparison of Global Vegetation Datasets, *Remote Sensing*, 5(10), 5193-5208.

Middleton, E. M., K. F. Huemmrich, D. R. Landis, T. A. Black, A. G. Barr, and J. H. McCaughey (2016), Photosynthetic efficiency of northern forest ecosystems using a MODIS-derived Photochemical Reflectance Index (PRI), *Remote Sensing of Environment*, 187, 345-366.

Peaucelle, M., P. Ciais, F. Maignan, M. Nicolas, S. Cecchini, and N. Viovy (2019), Representing explicit budburst and senescence processes for evergreen conifers in global models, *Agricultural and Forest Meteorology*, 266-267, 97-108.

Penuelas, J., M. F. Garbulsky, and I. Filella (2011), Photochemical reflectance index (PRI) and remote sensing of plant CO₂ uptake, *New Phytologist*, 191(3), 596-599.

Penuelas, J., J. A. Gamon, A. L. Fredeen, J. Merino, and C. B. Field (1994), Reflectance indices associated with physiological changes in nitrogen- and water-limited sunflower leaves, *Remote Sensing of Environment*, 48(2), 135-146.

Porcar-Castell, A., E. Tyystjarvi, J. Atherton, C. van der Tol, J. Flexas, E. E. Pfundel, J. Moreno, C. Frankenberg, and J. A. Berry (2014), Linking chlorophyll a fluorescence to photosynthesis for remote sensing applications: mechanisms and challenges, *Journal of experimental botany*, 65(15), 4065-4095.

Rahman, A. F., V. D. Cordova, J. A. Gamon, H. P. Schmid, and D. A. Sims (2004), Potential of MODIS ocean bands for estimating CO₂ flux from terrestrial vegetation: A novel approach, *Geophysical Research Letters*, 31(10).

Reichstein, M., et al. (2005), On the separation of net ecosystem exchange into assimilation and ecosystem respiration: review and improved algorithm, *Global Change Biology*, 11(9), 1424-1439.

Running, S. W., R. R. Nemani, F. A. Heinsch, M. S. Zhao, M. Reeves, and H. Hashimoto (2004), A continuous satellite-derived measure of global terrestrial primary production, *Bioscience*, 54(6), 547-560.

Ryu, Y., G. Lee, S. Jeon, Y. Song, and H. Kimm (2014), Monitoring multi-layer canopy spring phenology of temperate deciduous and evergreen forests using low-cost spectral sensors, *Remote Sensing of Environment*, 149, 227-238.

Shen, M., G. Zhang, N. Cong, S. Wang, W. Kong, and S. Piao (2014), Increasing altitudinal gradient of spring vegetation phenology during the last decade on the Qinghai-Tibetan Plateau, *Agricultural and Forest Meteorology*, 189-190, 71-80.

Verger, A., F. Baret, M. Weiss, I. Filella, and J. Peñuelas (2015), GEOCLIM: A global climatology of LAI, FAPAR, and FCOVER from VEGETATION observations for 1999-2010, *Remote Sensing of Environment*, 166, 126-137.

Walther, S., M. Voigt, T. Thum, A. Gonsamo, Y. Zhang, P. Kohler, M. Jung, A. Varlagin, and L. Guanter (2016), Satellite chlorophyll fluorescence measurements reveal large-scale decoupling of photosynthesis and greenness dynamics in boreal evergreen forests, *Glob Chang Biol*, 22(9), 2979-2996.

Wang, R., J. A. Gamon, C. A. Emmerton, K. R. Springer, R. Yu, and G. Hmimina (2020), Detecting intra- and inter-annual variability in gross primary productivity of a North American grassland using MODIS MAIAC data, *Agricultural and Forest Meteorology*, 281, 107859.

Wong, C. Y. S., and J. A. Gamon (2015a), The photochemical reflectance index provides an optical indicator of spring photosynthetic activation in evergreen conifers, *The New phytologist*, 206(1), 196-208.

Wong, C. Y. S., and J. A. Gamon (2015b), Three causes of variation in the photochemical reflectance index (PRI) in evergreen conifers, *The New phytologist*, 206(1), 187-195.

Wong, C. Y. S., P. D'Odorico, Y. Bhatena, M. A. Arain, and I. Ensminger (2019), Carotenoid based vegetation indices for accurate monitoring of the phenology of photosynthesis at the leaf-scale in deciduous and evergreen trees, *Remote Sensing of Environment*, 233, 111407.

Wu, C., et al. (2017), Land surface phenology derived from normalized difference vegetation index (NDVI) at global FLUXNET sites, *Agricultural and Forest Meteorology*, 233, 171-182.

Xia, J., et al. (2015), Joint control of terrestrial gross primary productivity by plant phenology and physiology, *Proceedings of the National Academy of Sciences of the United States of America*, 112(9), 2788-2793.

Zeng, Y., G. Badgley, B. Dechant, Y. Ryu, M. Chen, and J. A. Berry (2019), A practical approach for estimating the escape ratio of near-infrared solar-induced chlorophyll fluorescence, *Remote Sensing of Environment*, 232.

Zhang, C., I. Filella, D. J. Liu, R. Ogaya, J. Llusia, D. Asensio, and J. Penuelas (2017), Photochemical Reflectance Index (PRI) for Detecting Responses of Diurnal and Seasonal Photosynthetic Activity to Experimental Drought and Warming in a Mediterranean Shrubland, *Remote Sensing*, 9(11).

Zhang, Y., J. Joiner, S. H. Alemohammad, S. Zhou, and P. Gentine (2018), A global spatially contiguous solar-induced fluorescence (CSIF) dataset using neural networks, *Biogeosciences*, 15(19), 5779-5800.

Zhang, Y., N. C. Parazoo, A. P. Williams, S. Zhou, and P. Gentine (2020), Large and projected strengthening moisture limitation on end-of-season photosynthesis, *Proceedings of the National Academy of Sciences*, 117(17), 9216-9222.

Supporting References

Acosta, M., M. Pavelka, L. Montagnani, W. Kutsch, A. Lindroth, R. Juszczak, and D. Janous (2013), Soil surface CO₂ efflux measurements in Norway spruce forests: Comparison between four different sites across Europe - from boreal to alpine forest, *Geoderma*, 192, 295-303.

Anthoni, P. M., A. Knohl, C. Rebmann, A. Freibauer, M. Mund, W. Ziegler, O. Kolle, and E. D. Schulze (2004), Forest and agricultural land-use-dependent CO₂ exchange in Thuringia, Germany, *Global Change Biology*, 10(12), 2005-2019.

Arain, A. A., and N. Restrepo-Coupe (2005), Net ecosystem production in a temperate pine plantation in southeastern Canada, *Agricultural and Forest Meteorology*, 128(3-4), 223-241.

Berbigier, P., J. M. Bonnefond, and P. Mellmann (2001), CO₂ and water vapour fluxes for 2 years above Euroflux forest site, *Agricultural and Forest Meteorology*, 108(3), 183-197.

Chiesi, M., F. Maselli, M. Bindi, L. Fibbi, P. Cherubini, E. Arlotta, G. Tirone, G. Matteucci, and G. Seufert (2005), Modelling carbon budget of Mediterranean forests using ground and remote sensing measurements, *Agricultural and Forest Meteorology*, 135(1-4), 22-34.

Chu, H., et al. (2018), Temporal Dynamics of Aerodynamic Canopy Height Derived from Eddy Covariance Momentum Flux Data Across North American Flux Networks, *Geophysical Research Letters*, 45(17), 9275-9287.

Cook, B. D., et al. (2004), Carbon exchange and venting anomalies in an upland deciduous forest in northern Wisconsin, USA, *Agricultural and Forest Meteorology*, 126(3-4), 271-295.

DeForest, J. L., A. Noormets, S. G. McNulty, G. Sun, G. Tenney, and J. Chen (2006), Phenophases alter the soil respiration-temperature relationship in an oak-dominated forest, *International Journal of Biometeorology*, 51(2), 135-144.

Delpierre, N., D. Berveiller, E. Granda, and E. Dufrene (2016), Wood phenology, not carbon input, controls the interannual variability of wood growth in a temperate oak forest, *New Phytologist*, 210(2), 459-470.

Dragoni, D., H. P. Schmid, C. A. Wayson, H. Potter, C. S. B. Grimmond, and J. C. Randolph (2011), Evidence of increased net ecosystem productivity associated with a longer vegetated season in a deciduous forest in south-central Indiana, USA, *Global Change Biology*, 17(2), 886-897.

Dunn, A. L., C. C. Barford, S. C. Wofsy, M. L. Goulden, and B. C. Daube (2007), A long-term record of carbon exchange in a boreal black spruce forest: means, responses to interannual variability, and decadal trends, *Global Change Biology*, 13(3), 577-590.

Frank, J. M., W. J. Massman, B. E. Ewers, L. S. Huckaby, and J. F. Negrón (2014), Ecosystem CO₂/H₂O fluxes are explained by hydraulically limited gas exchange during tree mortality from spruce bark beetles, *Journal of Geophysical Research-Biogeosciences*, 119(6), 1195-1215.

Goldstein, A. H., N. E. Hultman, J. M. Fracheboud, M. R. Bauer, J. A. Panek, M. Xu, Y. Qi, A. B. Guenther, and W. Baugh (2000), Effects of climate variability on the carbon dioxide, water, and sensible heat fluxes above a ponderosa pine plantation in the Sierra Nevada (CA), *Agricultural and Forest Meteorology*, 101(2-3), 113-129.

Gough, C. M., B. S. Hardiman, L. E. Nave, G. Bohrer, K. D. Maurer, C. S. Vogel, K. J. Nadelhoffer, and P. S. Curtis (2013), Sustained carbon uptake and storage following moderate disturbance in a Great Lakes forest, *Ecological Applications*, 23(5), 1202-1215.

Goulden, M. L., G. C. Winston, A. M. S. McMillan, M. E. Litvak, E. L. Read, A. V. Rocha, and J. R. Elliot (2006), An eddy covariance mesonet to measure the effect of forest age on land-atmosphere exchange, *Global Change Biology*, 12(11), 2146-2162.

Gruenwald, T., and C. Bernhofer (2007), A decade of carbon, water and energy flux measurements of an old spruce forest at the Anchor Station Tharandt, *Tellus Series B-Chemical and Physical Meteorology*, 59(3), 387-396.

Irvine, J., B. E. Law, J. G. Martin, and D. Vickers (2008), Interannual variation in soil CO₂ efflux and the response of root respiration to climate and canopy gas exchange in mature ponderosa pine, *Global Change Biology*, 14(12), 2848-2859.

Knohl, A., E. D. Schulze, O. Kolle, and N. Buchmann (2003), Large carbon uptake by an unmanaged 250-year-old deciduous forest in Central Germany, *Agricultural and Forest Meteorology*, 118(3-4), 151-167.

Koskinen, M., K. Minkkinen, P. Ojanen, M. Kamarainen, T. Laurila, and A. Lohila (2014), Measurements of CO₂ exchange with an automated chamber system throughout the year: challenges in measuring night-time respiration on porous peat soil, *Biogeosciences*, 11(2), 347-363.

Kurbatova, J., C. Li, A. Varlagin, X. Xiao, and N. Vygodskaya (2008), Modeling carbon dynamics in two adjacent spruce forests with different soil conditions in Russia, *Biogeosciences*, 5(4), 969-980.

Lindauer, M., H. P. Schmid, R. Grote, M. Mauder, R. Steinbrecher, and B. Wolpert (2014), Net ecosystem exchange over a non-cleared wind-throw-disturbed upland spruce forest-Measurements and simulations, *Agricultural and Forest Meteorology*, 197, 219-234.

Marcolla, B., A. Pitacco, and A. Cescatti (2003), Canopy architecture and turbulence structure in a coniferous forest, *Boundary-Layer Meteorology*, 108(1), 39-59.

Migliavacca, M., M. Meroni, L. Busetto, R. Colombo, T. Zenone, G. Matteucci, G. Manca, and G. Seufert (2009), Modeling Gross Primary Production of Agro-Forestry Ecosystems by Assimilation of Satellite-Derived Information in a Process-Based Model, *Sensors*, 9(2), 922-942.

Monson, R. K., A. A. Turnipseed, J. P. Sparks, P. C. Harley, L. E. Scott-Denton, K. Sparks, and T. E. Huxman (2002), Carbon sequestration in a high-elevation, subalpine forest, *Global Change Biology*, 8(5), 459-478.

Montagnani, L., et al. (2009), A new mass conservation approach to the study of CO₂ advection in an alpine forest, *Journal of Geophysical Research-Atmospheres*, 114.

Nakai, T., Y. Kim, R. C. Busey, R. Suzuki, S. Nagai, H. Kobayashi, H. Park, K. Sugiura, and A. Ito (2013), Characteristics of evapotranspiration from a permafrost black spruce forest in interior Alaska, *Polar Science*, 7(2), 136-148.

Noormets, A., J. Chen, and T. R. Crow (2007), Age-dependent changes in ecosystem carbon fluxes in managed forests in northern Wisconsin, USA, *Ecosystems*, 10(2), 187-203.

Pilegaard, K., A. Ibrom, M. S. Courtney, P. Hummelshøj, and N. O. Jensen (2011), Increasing net CO₂ uptake by a Danish beech forest during the period from 1996 to 2009, *Agricultural and Forest Meteorology*, 151(7), 934-946.

Rey, A., E. Pegoraro, V. Tedeschi, I. De Parri, P. G. Jarvis, and R. Valentini (2002), Annual variation in soil respiration and its components in a coppice oak forest in Central Italy, *Global Change Biology*, 8(9), 851-866.

Ruehr, N. K., J. G. Martin, and B. E. Law (2012), Effects of water availability on carbon and water exchange in a young ponderosa pine forest: Above- and belowground responses, *Agricultural and Forest Meteorology*, 164, 136-148.

Sabbatini, S., N. Arriga, T. Bertolini, S. Castaldi, T. Chiti, C. Consalvo, S. N. Djomo, B. Gioli, G. Matteucci, and D. Papale (2016), Greenhouse gas balance of cropland conversion to bioenergy poplar short-rotation coppice, *Biogeosciences*, 13(1), 95-113.

Suni, T., J. Rinne, A. Reissell, N. Altimir, P. Keronen, U. Rannik, M. Dal Maso, M. Kulmala, and T. Vesala (2003), Long-term measurements of surface fluxes above a Scots pine forest in Hyytiälä, southern Finland, 1996-2001, *Boreal Environment Research*, 8(4), 287-301.

Tedeschi, V., A. Rey, G. Manca, R. Valentini, P. G. Jarvis, and M. Borghetti (2006), Soil respiration in a Mediterranean oak forest at different developmental stages after coppicing, *Global Change Biology*, 12(1), 110-121.

Thum, T., T. Aalto, T. Laurila, M. Aurela, P. Kolari, and P. Hari (2007), Parametrization of two photosynthesis models at the canopy scale in a northern boreal Scots pine forest, *Tellus Series B-Chemical and Physical Meteorology*, 59(5), 874-890.

Urbanski, S., C. Barford, S. Wofsy, C. Kucharik, E. Pyle, J. Budney, K. McKain, D. Fitzjarrald, M. Czikowsky, and J. W. Munger (2007), Factors controlling CO₂ exchange on timescales from hourly to decadal at Harvard Forest, *Journal of Geophysical Research-Biogeosciences*, 112(G2).

Valentini, R., P. DeAngelis, G. Matteucci, R. Monaco, S. Dore, and G. E. S. Mugnozza (1996), Seasonal net carbon dioxide exchange of a beech forest with the atmosphere, *Global Change Biology*, 2(3), 199-207.

Zeller, K. F., and N. T. Nikolov (2000), Quantifying simultaneous fluxes of ozone, carbon dioxide and water vapor above a subalpine forest ecosystem, *Environmental Pollution*, 107(1), 1-20.

Zielis, S., S. Etzold, R. Zweifel, W. Eugster, M. Haeni, and N. Buchmann (2014), NEP of a Swiss subalpine forest is significantly driven not only by current but also by previous year's weather, *Biogeosciences*, 11(6), 1627-1635.